JOURNAL OF GEOPHYSICAL RESEARCH, VOL. 115, D03105, doi:10.1029/2009JD012081, 2010

Carbon dioxide retrievals from Atmospheric Chemistry Experiment solar occultation measurements

Curtis P. Rinsland,[1] Linda S. Chiou,[2] Chris Boone,[3] and Peter Bernath[3,4]

Received 17 March 2009; revised 28 September 2009; accepted 2 October 2009; published 3 February 2010.

[1] The Atmospheric Chemistry Experiment (ACE) satellite (SCISAT-1) was launched into an inclined orbit on 12 August 2003 and is now recording high signal-to-noise 0.02 cm^{-1} resolution solar absorption spectra covering 750–4400 cm^{-1} (2.3–13 μm). A procedure has been developed for retrieving average dry air CO_2 mole fractions (X_{CO_2}) in the altitude range 7–10 km from the SCISAT-1 spectra. Using the N_2 continuum absorption in a window region near 2500 cm^{-1}, altitude shifts are applied to the tangent heights retrieved in version 2.2 SCISAT-1 processing, while cloudy or aerosol-impacted measurements are eliminated. Monthly mean X_{CO_2} covering 60°S to 60°N latitude for February 2004 to March 2008 has been analyzed with consistent trends inferred in both hemispheres. The ACE X_{CO_2} time series have been compared with previously reported surface network measurements, predictions based on upper tropospheric aircraft measurements, and space-based measurements. The retrieved X_{CO_2} from the ACE-FTS spectra are higher on average by a factor of 1.07 ± 0.025 in the Northern Hemisphere and by a factor of 1.09 ± 0.019 on average in the Southern Hemisphere compared to surface station measurements covering the same time span. The ACE-derived trend is ~0.2% per year higher than measured at surface stations during the same observation period.

Citation: Rinsland, C. P., L. S. Chiou, C. Boone, and P. Bernath (2010), Carbon dioxide retrievals from Atmospheric Chemistry Experiment solar occultation measurements, *J. Geophys. Res.*, *115*, D03105, doi:10.1029/2009JD012081.

1. Introduction

[2] At present, there are no global satellite-based measurements of carbon dioxide (CO_2) profiles despite a continuing increase as a function of time with important implications for climate change [*Intergovernmental Panel on Climate Change*, 2007]. Inversion of atmospheric data for the estimation of CO_2 surface sources and sinks relies primarily on the availability of atmospheric remote sensing and ground-based surface network observations. However, current observations are sparse, particularly over ocean regions, the tropics and subtropics, and in the Southern Hemisphere. Recent studies demonstrate that an average precision of 2.5 ppm (1 ppm = 10^{-6}), less than 0.7% of 375 ppm (the value of CO_2 dry air mole fraction (X_{CO_2}) circa 2009), would be required from monthly averaged column data on a 8 × 10 km^2 footprint to achieve comparable constraints on surface sources as compared to those from the existing flask network [*Rayner and O'Brien*, 2001]. Global column measurements of X_{CO_2} with a precision of 1 ppm (0.3%) are required to quantify the variation of sources and sinks and improve future climate forecasts [*Miller et al.*, 2007]. *Pak and Prather* [2001] concluded that satellite observations of upper tropospheric CO_2 profiles have the potential to provide a constraint for deriving net carbon fluxes, although a precision of about 1% is needed. That work suggested a Fourier Transform Spectrometer (FTS) would offer the potential for such measurements, taking advantage of high signal-to-noise and also simultaneous profile measurements of a large number of additional species down to an altitude of about 5 km.

[3] The first dedicated spaceborne remote sensing missions to measure CO_2 were planned to begin in early 2009 with the launch of the Greenhouse Gases Observing Satellite (GOSAT) by Japan Aerospace Exploration Agency (JAXA) and NASA's Orbiting Carbon Observatory (OCO). GOSAT was successfully launched on 23 January 2009 with initial functional testing and validation scheduled to be completed 3 months after launch by the Japanese National Institute of Environmental Studies and the Ministry of the Environment (MOE). GOSAT uses a FTS with high-optical throughput, spectral resolution, and wide spectral coverage. The instrument measures both CO_2 and CH_4 from thermal infrared and reflected sunlight observations (0.76–15 μm) [*Hamazaki et al.*, 2005]. The OCO mission [*Crisp et al.*, 2004] had a primary goal of measuring precise X_{CO_2} columns in the near infrared from low Earth orbit and quantifying CO_2 sources and sinks globally from the measured columns. The OCO mission was designed to use three bore-sighted, long-slit nadir-viewing near-infrared

[1]NASA Langley Research Center, Hampton, Virginia, USA.
[2]Science Systems and Applications, Inc., Hampton, Virginia, USA.
[3]Department of Chemistry, University of Waterloo, Waterloo, Ontario, Canada.
[4]Also at Department of Chemistry, University of York, York, UK.

0148-0227/10/2009JD012081$09.00

grating spectrometers. However, OCO failed to reach orbit after its launch on 24 February 2009.

[4] High precision X_{CO_2} measurements are required because of the difficulty in disentangling the contributions of different sources and sinks [*Tans et al.*, 1990], the presence of clouds and/or aerosols, the effects of CO_2 source signal dilution with height, and near uniform X_{CO_2} background profile distant from major source/sink regions. Inversions that provide CO_2 fluxes are sensitive to assumptions of transport [*Law et al.*, 1996; *Fan et al.*, 1998] with currently limited capability in quantifying regional distributions of sources and sinks from atmospheric measurements due to limited sampling [*Fan et al.*, 1998; *Chevallier et al.*, 2005; *Tiwari et al.*, 2006]. Transport out of the boundary layer to the free troposphere is not well understood and may be key to identifying sink regions [*Strow and Hannon*, 2008]. Knowledge of the present oceanic and terrestrial uptake would have immediate implications for a greenhouse gas emission policy [*Tans et al.*, 1996].

[5] The potential utility of CO_2 tropospheric solar occultation profile measurements with a FTS from inclined-orbit measurements for quantifying CO_2 source distributions has been assessed [*Patra et al.*, 2003], assuming a realistic cloud distribution. Those results suggest that such observations would be valuable if sufficient precision is achieved and in particular would help constrain source flux uncertainties for the tropical lands with no existing observations. The Atmospheric Chemistry Experiment (ACE) [*Bernath et al.*, 2005] has the potential to obtain high-precision measurements directly relevant to carbon cycle science objectives, given quantitative procedures for cloud and aerosol detection. A previous study investigated the feasibility of retrieving CO_2 profiles in the 5–25 km altitude range from the ACE-FTS [*Foucher et al.*, 2009], working with synthetic spectra, but also providing estimates for retrievals based on real ACE-FTS data. The importance of potential bias in CO_2 retrievals due to errors in the temperature and the nitrogen pressure-induced coefficients also was noted.

[6] Seasonal and latitudinal variations of CO_2 mid-tropospheric zonal mean mixing ratios [*Chahine et al.*, 2008] and a 4 year climatology of lower tropospheric clear sky ocean-only CO_2 measurements between ±60° latitude [*Strow and Hannon*, 2008] have been reported recently from nadir AIRS measurements. Measurements were limited to the Northern Hemisphere and low latitudes in the Southern Hemisphere. A climatology of lower tropospheric SCIAMACHY/ENVISAT X_{CO_2} total column measurements obtained between 2003 and 2005 primarily in the Northern Hemisphere over land have been used to measure seasonal and latitudinal averages and determine an increase rate for that time period [*Buchwitz et al.*, 2007].

2. ACE Measurements

[7] The ACE satellite was launched on 12 August 2003 into a 74° circular orbit at 650 km altitude and has been in operation for science measurements since February 2004, providing up to 30 solar occultations per day [*Bernath et al.*, 2005]. The ACE orbit is optimized for high-latitude coverage in both hemispheres. Measurements are recorded with the ACE-FTS, a UV-visible spectrometer, and two visible imagers below about 150 km altitude. The ACE-FTS records spectra at 0.02 cm^{-1} spectral resolution (maximum optical path difference (OPD) of ±25 cm) from 750 to 4400 cm^{-1}. Full resolution spectra are recorded in 2 s with an altitude spacing determined by the scan time, typically 3–4 km, varying from 2 km for long, high beta angle (angle between the plane of the orbit and the Sun) occultations and up to 6 km for zero beta angle occultations. As a result of refraction, tangent altitude spacing is typically less than 2 km in the troposphere. The FTS has a circular field of view (FOV) 1.25 mrad (10^{-3} radian) in diameter, which corresponds to 3–4 km at the limb in the absence of refraction. Photovoltaic detectors with near linear response produce a signal-to-noise ratio of greater than 300:1 throughout most of the spectral range. Low Sun solar occultation spectra are divided by exo-atmospheric solar spectra from the same occultation to remove nontelluric absorptions yielding measurements between about 85°N and 85°S latitude. Middle and low latitudes are recorded only over limited time spans because of the high inclination of the satellite's orbit. All occultations within ±60° latitude with the exception of those inside or on the edge of the polar vortex have been included in our analysis covering February 2004 to March 2008.

3. Retrievals

[8] Pressure-temperature profiles for each occultation have been retrieved as part of the procedure for analysis of the ACE-FTS spectra. The assumptions for that analysis, the a priori profile for X_{CO_2}, and its trend versus time are described in the paper by *Boone et al.* [2005]. Versions 1.0 through 2.2 processing are described in that paper, where version 2.2 is the current set of ACE-FTS results. The model described in that paper assumes a linear increase in X_{CO_2} with time based on the equation adopted previously for analysis and retrievals from Halogen Occultation Experiment (HALOE) measurements.

[9] In the version 2.2 ACE-FTS retrievals, X_{CO_2} in the middle atmosphere is assumed constant, fixed to the value calculated from the model. An additional 5.5 ppm is assumed in the troposphere. No provision is made for the variation in X_{CO_2} with location and season. At high altitudes (above ~60 km), CO_2 volume mixing ratio (VMR) is fitted, employing an empirical function to smooth out unphysical oscillations. Pressure and temperature are retrieved down to 12 km. Below 12 km, pressure and temperature are fixed to the "reanalysis" data from the Canadian Meteorological Centre (CMC).

[10] Over 12,500 occultations have been acquired by ACE since launch with current ACE (version 2.2) profiles determined assuming HITRAN 2004 spectroscopic parameters [*Rothman et al.*, 2005]. However, a high fraction of the ACE measurements are significantly affected by cloud attenuation at middle and upper tropospheric altitudes. We developed a cloud identification procedure using measurements in a microwindow to eliminate those scenes from the ACE database as well as a procedure to improve the precision of X_{CO_2} retrievals from the remaining ACE spectra based on analysis of a window with continuum absorption by the infrared fundamental band of N_2. We next describe

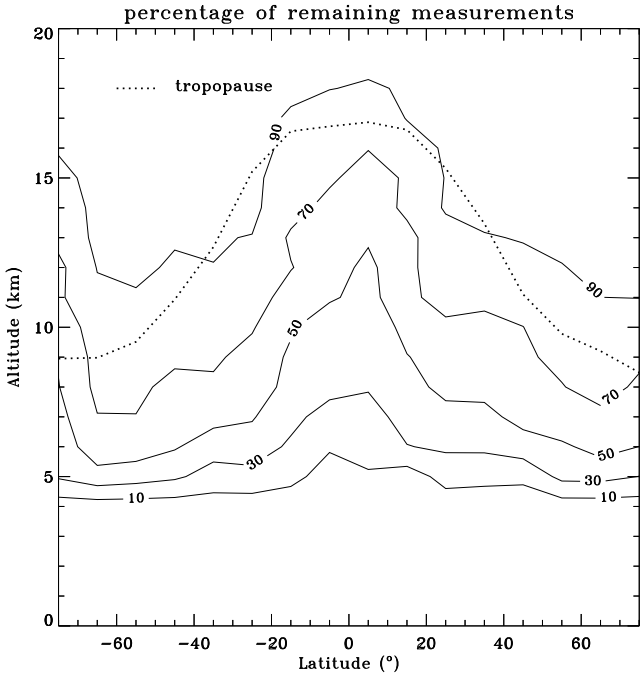

Figure 1. Fraction of remaining ACE measurements versus latitude assuming the cloud rejection criterion and the microwindow at 956.7–957.0 cm^{-1}. The dotted line shows the approximate location of the tropopause as a function of latitude based on U.S. National Center for Environmental Prediction (NCEP) measurements.

the procedure for identifying and excluding ACE measurement scenes significantly impacted by cloud extinction.

[11] A single microwindow (956.7–957.0 cm^{-1}) was chosen for the detection of clouds or aerosol extinction [*Rinsland et al.*, 1998]. As noted in that work, radiative transfer calculations with known molecular lines, absorption cross sections, and a reference set of vertical gas concentration profiles predict a transmittance of 0.99 and 0.97 above 150 mbar (~14 km altitude). We analyzed all spectra in the version 2.2 ACE-FTS database at 60°N to 60°S latitude applying a criterion for each occultation that reaches a tangent height of 10 km or below. We assume that if the transmission in the measured spectrum divided by that calculated for the simulated spectrum in the window is less than 0.8, then the occultation is cloud impacted and not considered for further analysis. Figure 1 provides a plot of the fraction of remaining measurements versus latitude after adopting this cloud/aerosol rejection criterion. Measurements penetrate on average approximately 5 km below the tropopause at all latitudes, a result that is consistent with a previous study based on Stratospheric Aerosol and Gas Experiment (SAGE) II 1.02 μm observations [*Wang et al.*, 1998]. Profiles of X_{CO_2} were retrieved from the remaining measurements after applying a vertical offset to the tangent altitudes obtained from ACE version 2.2 processing. We next briefly describe the procedure we adopted.

[12] As pointed out previously [*Foucher et al.*, 2009], two main difficulties for retrieving CO_2 from ACE spectra are: (a) accurate determination of the instrument pointing parameters (tangent heights) and (b) sensitivity of retrieved CO_2 to pressure/temperature profiles. Studies by *Rinsland et al.* [2004] using atmospheric trace molecule spectroscopy (ATMOS) solar occultation FTS spectra recorded at 0.01 cm^{-1} resolution indicated that analysis of continuum pressure-induced absorption by N_2 and CO_2 in the window region 2395–2525 cm^{-1} could help achieve the goal of precise determination of stratospheric densities from occultation measurements. Thus, we have implemented a procedure to determine the altitude shift to apply to version 2.2 ACE tangent heights as our means to resolve the difficulty (a) mentioned above.

[13] Continuum absorption by the pressure-induced fundamental band of molecular nitrogen at 4.3 μm was studied previously based on FTS measurements [*Rinsland et al.*, 1989, 2004]. The absorption is significant over a wide altitude range and increases with the square of the density. Collision-induced absorption coefficients for N_2 (cm^{-1} atm^{-1}) and their dependence with temperature have been reported for 2125 to 2600 cm^{-1} [*Lafferty et al.*, 1996, Table 1]. Continuum absorption by CO_2 also occurs in the window region, but its absorption is negligible in the 2500.6–2500.9 cm^{-1} interval selected for the current analysis [*Rinsland et al.*, 2004, Figure 2]. The window contains a weak CH_4 line at 2500.7616 cm^{-1} with a ~5% line center absorption depth at 6.6 km tangent altitude. We determined the vertical offset to apply to individual version 2.2 spectra based on this window by comparing measured and calculated transmittances in the 7–12 km altitude range. No vertical offset was applied to the version 2.2 tangent heights above 12 km altitude. In the Northern Hemisphere, the average values of the applied tangent height shifts are in the range of −0.19 km to 0.34 km between 7 km and 10 km. For the Southern Hemisphere, they range from −0.25 km to 0.37 km.

[14] The ACE spectra obtained after the altitude offset is applied were analyzed with a multimicrowindow Levenberg-Marquardt nonlinear least squares global-fitting technique [*Carlotti*, 1988]. Concentration profiles were retrieved from simultaneous fits to a sequence of spectra recorded in the limb-viewing mode. Microwindow regions in all of the spectra from a given occultation were fitted simultaneously over a preselected altitude range with an assumed pressure-temperature profile to derive X_{CO_2} and interfering species based on an assumed set of molecular spectroscopic parameters and a set of a priori profiles. Examples of studies using this approach are presented by *Rinsland et al.* [1987, 1991]. The Levenberg-Marquardt nonlinear least squares multimicrowindow analysis approach is the same as is used to retrieve profiles from ACE-FTS spectra [*Boone et al.*, 2005].

[15] Figure 2 illustrates fitting results for the five selected wave number intervals for the sunrise occultation sr11055 at 6.48 km used to derive X_{CO_2} from the ACE spectra. The windows span 2615–2635 cm^{-1} and were selected for the retrievals based on those used for ACE retrievals [*Boone et al.*, 2005, Table 2] primarily because the lines are relatively insensitive to temperature, and they can be used for occultations at altitudes as low as 5 km with minimal molecular interferences. We fitted CH_4 and CO_2 in the three lower wave number intervals. Only CO_2 was fitted in the two higher wave number windows. Note that the lines in these windows belong to a subsidiary isotopologue of CO_2 ($^{16}O^{12}C^{18}O$). There is an inconsistency between these lines

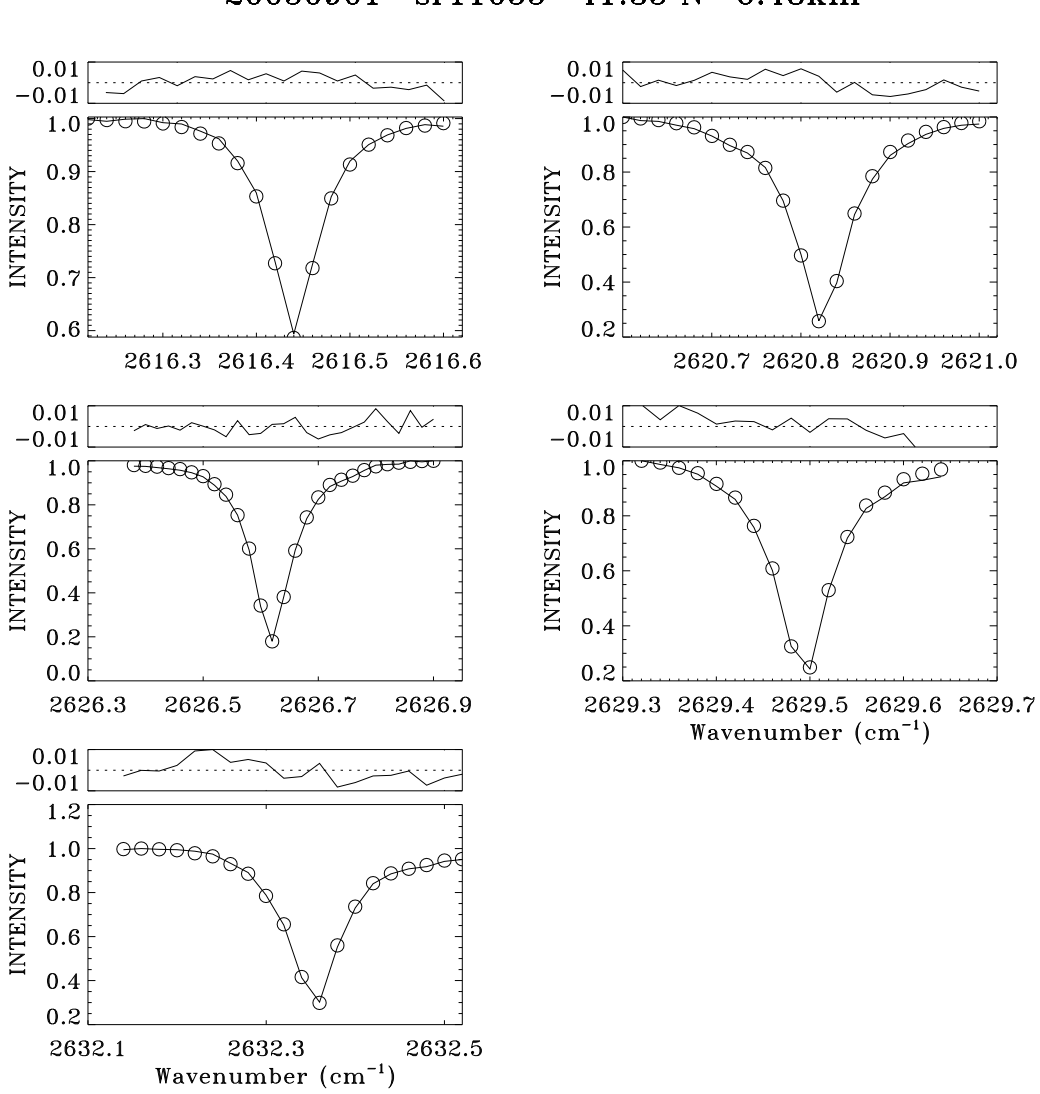

Figure 2. Sample spectrum and fit obtained from analysis of CO_2 with the five selected microwindows. In each microwindow, (top) the location and adjusted tangent altitude of the measured spectrum and (bottom) the residuals on an expanded scale from the normalized measured spectrum above the measured spectrum are shown. The tangent altitude in the ACE version 2.2 database of the spectrum is 6.631 km.

and lines from the main isotopologue ($^{16}O^{12}C^{16}O$), likely a combination of intensity errors for these weak lines and atmospheric fractionation. The $^{12}C^{16}O^{18}O$ species is a stable isotopologue with the $^{18}O/^{16}O$ ratio in atmospheric CO_2 influenced primarily by oxygen exchange with water in soils and plants [*Francey and Tans*, 1987]. Using measurements between 12 and 20 km, *Boone et al.* [2005] determined a discrepancy of 3.5% between these $^{12}C^{16}O^{18}O$ lines and lines from the main isotopologue. Intensities for the $^{12}C^{16}O^{18}O$ lines were thus increased by 3.5% whenever they were employed in the ACE-FTS pressure/temperature retrievals. The value of this "correction factor" has been adjusted to 4.3% for the next processing version of the ACE-FTS (version 3.0).

[16] ACE-FTS spectra are unapodized, but the instrument suffers from a self-apodization of unknown origin [*Boone et al.*, 2005]. In order to fit lines to the noise level in the spectra, it is necessary to introduce an empirical function to account for self-apodization effects. The analysis here adopts an empirical model that retains the nominal ACE-FTS optical path difference (OPD) but multiplies the ACE-FTS modulation function by a triangular function that decreases linearly from 1.0 at zero OPD to a best fit value at the maximum OPD. The form of the empirical function used in the official ACE-FTS processing was different [*Boone et al.*, 2005], mostly because the official processing needed to account for the variation with wave number of the self-apodization effects. The simple function assumed in this work is sufficient to account for instrument self-apodization effects over the narrow wave number range employed in this study.

[17] Table 1 provides a list of the most important sources of random and systematic error and provides estimates of

Table 1. Random and Systematic Sources of Error in Retrieval of 7–10 km X_{CO_2}[a]

Error Source	Error Type	Relative Uncertainty (%)
Finite signal to noise	R	<1
Temperature profile	R	1
Retrieval algorithm	S	1
Nitrogen continuum absorption coefficients	S	2
CO_2 line intensities	S	4
Aerosol	S	<1
CO_2 isotopologue correction	S	<1
Uncertainty in the ACE-FTS ILS	S	<1
Uncertainty in the vertical altitude shift	S	<1

[a]S, systematic; R, random; ILS is the instrument line shape function.

uncertainties in the ACE-retrieved 7–10 km X_{CO_2}. Random errors are much less important than systematic errors because of the high signal-to-noise ratio of the ACE-FTS spectra. Random errors due to the finite signal-to-noise ratio of the ACE spectra is further reduced by averaging the transmittance over the 2500.6–2500.9 cm^{-1} interval, the window region used to estimate the contribution of the N_2 continuum to the spectrum. Random noise is also reduced by reporting monthly mean X_{CO_2} over 7–10 km altitude. Temperature is classified as a random source of error, with validation studies indicating that agreement of version 2.2 temperatures with other sensors is typically better than 2 K in the stratosphere and upper troposphere [*Sica et al.*, 2008]. The magnitude of seven sources of potential systematic error were considered and are discussed below.

[18] 1. The retrieval algorithm used in the present study is a potential source of systematic error. It was used in similar retrievals of ATMOS spectra [*Rinsland et al.*, 1987, 1989, 1991] and ACE spectra [*Rinsland et al.*, 2007, 2010] and on the basis of those results and use in comparison with model predictions, we estimate the bias in retrieving molecular profiles as 1%.

[19] 2. Line intensities for the CO2 bands in the region were derived from 0.01 cm^{-1} resolution laboratory spectra [*Malathy Devi et al.*, 1984]. The measurements were recorded at room temperature and low pressure in a 6 m base path White cell. The gas sample was a 99.995% minimum purity CO_2 sample. The isotopic composition of the sample was not measured. The intensities from that work [*Malathy Devi et al.*, 1984] are a factor of 1.15 higher than those from an earlier lower resolution laboratory study [*Hoke and Shaw*, 1982, Table 1], though intensities from an earlier grating spectrometer band intensities were reported as in agreement [*Malathy Devi et al.*, 1984]. The line intensities reported earlier [*Hoke and Shaw*, 1982] were calculated assuming the isotopic abundances in naturally occurring CO_2, which was used for collecting the measurement sample. The above-cited studies suggest errors in the assumed intensities may introduce errors of up to 15%. To determine which set of CO_2 line intensities is more accurate, a study was undertaken with solar absorption data measured by the Kitt Peak FTS (31.9°N latitude, 111.6°W longitude, 2.09 km altitude). Daily average 2.09–10 km altitude X_{CO_2} from 1977 to 2008 were derived from analysis of the spectral region near 2625 cm^{-1} with the SFIT2 version 3.93 algorithm, which is based on the optimal estimation method [*Rodgers*, 1990] modified with a semi-empirical implementation [*Parrish et al.*, 1992; *Connor et al.*, 1995]. The spectroscopic parameters from the HITRAN 2004 database [*Rothman et al.*, 2005] were assumed in the retrievals. The comparison shows agreement between the Kitt Peak daily mean X_{CO_2} and monthly mean measurements from two surface stations (BME at 32.37°N latitude, 64.65° longitude and WIS at 31.13°N latitude, 34.88° longitude) at similar latitude. The ratio of the Kitt Peak monthly means for the 2.09–10 km altitude range to the monthly mean measurements from the BME and WIS stations for nearly the same time span during December 1995 to June 2005 are 1.019 ± 0.024 and 1.017 ± 0.02, respectively. A total of 58 monthly means from Kitt Peak based on measurements from five microwindow with spectral intervals similar to those used for the ACE retrievals were compared with 115 monthly means from the BME station and 115 monthly means from the WIS station. X_{CO_2} from three windows spanning 3203–3326 cm^{-1} are on average 2.2% lower than those from the five windows used for the retrievals reported in this work. On the basis of these comparisons and the offset applied in the version 2.2 ACE-FTS pressure/temperature retrievals for these lines, we estimated the systematic error in the assumed line intensities as 4%.

[20] 3. Error in the assumed temperature-dependent absorption coefficients is a source of potential bias. Our analysis assumes temperature-dependent absorption coefficients [*Lafferty et al.*, 1996] covering 2125–2600 cm^{-1} predicted from measurements recorded in the 0–10 atm and 230–300 K pressure ranges, respectively. FTS measurements of pure N_2 recorded at 0.5 cm^{-1} spectral resolution and N_2 absorption coefficient measurements were combined with grating spectrometer measurements of N_2 and O_2 mixtures at 193–297 [*Menoux et al.*, 1993] as both were found to be consistent within their experimental uncertainties. The empirical model used to analyze the combined set yielded the predicted absorption coefficient (cm^{-1} atm^{-1}) and its dependence with temperature in increments of 5 cm^{-1}. The region from 2460 to 2560 cm^{-1} is important as it contains window intervals dominated by N_2 continuum absorption that provide transmissions potentially useful for retrievals of vertical offsets at upper tropospheric and lower stratospheric altitudes. We tested the consistency of the altitude shifts deduced from the ACE spectra by comparing shifts determined from 10 clear sky occultations covering the altitude range, applying the altitude shifts as described previously. Altitude shifts from two microwindows (2500.6–2500.9 and 2522.9–2522.95 cm^{-1}) agreed to 0.4 km, but both intervals are in regions that are sensitive to errors in the predicted temperature dependence of the N_2 absorption coefficient [*Lafferty et al.*, 1996, Table 1]. We adopted 3% as the relative uncertainty based on these comparisons, the sensitivity due to differences in the reported measurement sets [*Lafferty et al.*, 1996, Figures 5 and 6], possible bias due to error in the empirical model adopted to calculate the temperature-dependent absorption coefficients [*Lafferty et al.*, 1996, equations 4 and 8], and uncertainties in ACE upper tropospheric temperatures. More recent FTS integrated band intensity measurements [*Baranov et al.*, 2005] derived at temperatures up to 360 K

are about 3% lower than previous results but about 1% larger than reported by *Menoux et al.* [1993]. New low-temperature measurements of N_2 collision-induced absorption coefficients at 5 μm are planned (Y. Baranov, National Institute of Standards and Technology, private communication, 2009). The tangent height retrieval error (in km) for N_2 continuum absorption in the 5–10 km altitude range as a function of microwindow width (cm^{-1}) derived assuming the absorption coefficients of *Lafferty et al.* [1996] yielded an uncertainty of 0.035 cm^{-1} [*Foucher et al.*, 2009, Table 6]. As our primary N_2 window is 0.3 cm^{-1} wide, a retrieval error of 0.3% was estimated. The corresponding uncertainty in the X_{CO_2} is 0.1%. However, this estimate does not take into account the much larger spectroscopic uncertainties. We adopted 2% as the estimated uncertainty in X_{CO_2} due to uncertainty in the N_2 pressure-induced fundamental band absorption coefficients near 2500 cm^{-1}.

[21] 4. The HITRAN database incorporates assumed terrestrial isotopologue abundances for each molecular species as defined by *De Bièvre et al.* [1984]. We have assumed those values. As the relative abundances of different CO_2 isotopologues vary with ecosystem and such differences are not yet well understood, but they are recognized as potential indicators for identifying different emission sources. Deviations from the assumed HITRAN isotopologue value are a potential source of systematic error in the ACE CO_2 retrievals. As mentioned earlier, lines of $^{16}O^{18}O^{16}O$ are used in the low-altitude retrieval of CO_2, and when they are combined with those for $^{16}O^{12}C^{18}O$ and the $^{16}O^{12}C^{16}O$ at 12–20 km a bias occurs. On the basis of those results and other studies [*Francey and Tans*, 1987; *Allison and Francey*, 2007; *Nakazawa et al.*, 1997], we estimate atmospheric fractionation among different CO_2 stable isotopologues may introduce a systematic error of <1%.

[22] 5. Extinction due to aerosols contributes to the absorption along the long paths measured during solar occultation observations, and in the past significant infrared extinction has been measured shortly after major volcanic eruptions [e.g., *Rinsland et al.*, 1994; *Kent et al.*, 1995]. Currently, aerosol levels are very low, and absorption by aerosols is much less significant in the infrared than the visible. Additionally, the spectral region for measurement of pressure-induced absorption by nitrogen is located in a region of low-infrared extinction [*Rinsland et al.*, 1994]. We assume an upper limit of 1% as the potential bias introduced by not including aerosol extinction in our retrievals. More recently, active remote sensing measurements of aerosols and clouds have become available with lidar techniques with global distributions [*Winker et al.*, 2007].

[23] 6. As mentioned earlier, the approach used for fitting the ACE-FTS ILS differs from that adopted in the standard processing of atmospheric spectra, though there is agreement that the measured ILS is broader than predicted with the nominal parameters for the ACE ILS. As both studies reach a similar conclusion, we estimate an upper limit for the impact of the error in retrieving X_{CO_2} at 7–10 km as less than 1%.

[24] 7. Potential bias in determining the altitude shift is linked to systematic errors in the assumed N_2 continuum absorption coefficients (error source 3). The window for determining the vertical altitude shift is relatively narrow (2500.6–2500.9 cm^{-1}), and we have assumed the altitude shift above an altitude of 12 km is zero. Considering only these two factors, we estimate a potential error in X_{CO_2} from both as less than 1%.

4. Results

[25] The 7–10 km altitude range for the retrievals was chosen to reach as low as possible but retain sufficient observations to allow measurement of statistically significant seasonal changes in X_{CO_2} and its trend in both hemispheres. The time series of monthly averaged measurements was fitted with the expression

$$C_A = a_0 + a_1(t - t_0) + a_2 \cos(2\pi(t - t_0 - \varphi)), \qquad (1)$$

where C_A is the X_{CO_2} at time t, a_0 is the mean X_{CO_2} at time t_0, a_1 is the trend, a_2 is the amplitude of the seasonal cycle, and φ is the phase corresponding to the seasonal cycle maximum. Measurements of X_{CO_2} and its trend are limited primarily to those from surface station sampling sites. Equation (1) is an approximation.

[26] Figure 3 compares monthly mean ACE X_{CO_2} at 7–10 km altitude with no altitude shifts and monthly average Earth System Research Laboratory (ESRL) NOAA (National Oceanic and Atmospheric Administration) surface measurements for the same time period. Measurements for 0–60°N latitude are in the upper panel and those for 0–60°S latitude are in the lower panels with residuals (measured minus calculated monthly averaged X_{CO_2}) on an expanded vertical scale. Each individual occultation that results in a successful retrieval was used to perform linear interpolation onto 1 km altitude spacing before calculating average X_{CO_2} for the 7–10 km layer. Open triangles in Figure 3 display ACE monthly mean X_{CO_2} measurements and the vertical lines indicate their standard deviations. The regression fit with equation (1) is shown as a solid curve and the slightly tilted straight line represents the constant term plus the trend term. Listings of the locations and altitudes of the Northern and Southern hemisphere NOAA/ESRL surface station used for comparison with ACE measurements are provided in Tables 2 and 3, respectively. The station codes are shown in Figure 3.

[27] Figure 4 shows the comparison of the Northern Hemisphere (0–60°N latitude) and Southern Hemisphere (0–60°S latitude) monthly mean X_{CO_2} time series at 7–10 km altitude when ACE-FTS tangent heights were adjusted through the analysis with the N_2 continuum prior to the retrievals. As in Figure 3, open triangles represent the measurements and vertical lines indicate their 1-sigma statistical uncertainty with a solid curve indicating the best fit to the time series assuming equation (1) and residuals displayed above on an expanded vertical scale. The time series are again compared with the NOAA/ESRL monthly mean time series for the same time period (same as in Figure 3). As can be seen from Figure 4, a significant seasonal variation occurs whereas none is significant in Figure 3, reflecting the use of a nonseasonally varying a priori profile below middle atmo-

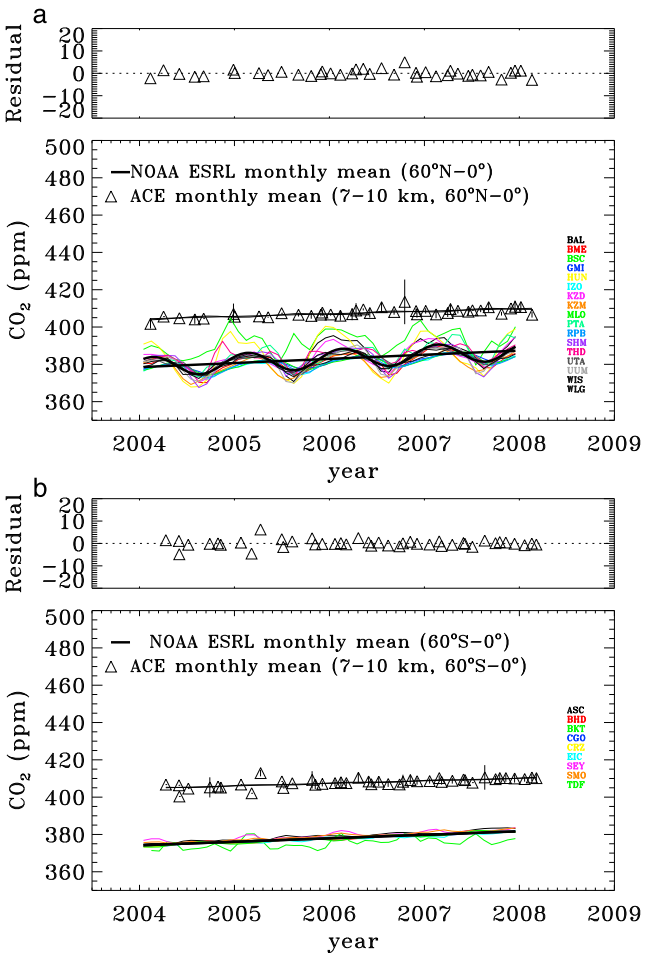

Figure 3. Comparison of ACE monthly mean X_{CO_2} at 7–10 km altitude at latitudes of (a) 0–60°N and (b) 0–60°S latitude. No altitude shifts have been applied to the observations (see text for details). Open triangles and vertical lines indicate the monthly mean dry air mole fraction and its standard deviation, respectively. Measured minus calculated residuals derived with equation (1) (solid line) are shown above on an expanded vertical scale. The ACE time series are compared with monthly average X_{CO_2} surface station measurements in both hemispheres. Thick lines show linear trend fits from the NOAA ESRL monthly mean regression fits. Colored thin lines connect monthly means from individual stations. Latitude, longitude, and elevation of NOAA ESRL stations with station codes are shown to the right.

spheric altitudes in the version 2.2 ACE temperature/pressure retrievals [*Boone et al.*, 2005].

5. Discussion

[28] Table 4 provides best fit results to ACE monthly average time series with equation (1) for Northern Hemisphere (0–60°N latitude), the Southern Hemisphere (0–60°S latitude), and their 1-sigma statistical uncertainties. The average X_{CO_2}, its trend, and corresponding 1-sigma uncertainty obtained from a fit with equation (1) to the NOAA/ESRL monthly mean in situ X_{CO_2} measurements

Table 2. Station Codes, Locations, and Altitudes of the Northern Hemisphere NOAA/ESRL Surface Stations Used in the Study

Station	Latitude (°N)	Longitude (°)	Altitude (m)
BAL	55.50	16.67	7.0
BME	32.37	−64.65	30
BSC	44.17	28.68	3
GMI	13.43	144.78	2
HUN	46.95	16.65	344
IZO	28.30	−16.48	2300
KZD	44.45	75.57	412
KZM	43.25	77.88	2519
MLO	19.53	−155.58	3397
PTA	38.95	−123.73	55
RPB	13.17	−59.45	3
SHM	52.72	174.10	40
THD	41.05	−124.15	107
UTA	39.90	−113.72	1320
UUM	44.45	111.10	914
WIS	31.13	34.88	400
WLG	36.27	100.92	3810

covering the same time span are also reported. The ACE monthly measurements are on average a factor of 1.07 ± 0.025 higher in the Northern Hemisphere and a factor of 1.09 ± 0.019 higher than the NOAA ESRL Southern Hemisphere surface station measurements.

[29] The mean and standard deviation of ACE X_{CO_2} for the Northern Hemisphere covering 44 months is 412.35 ± 7.20 ppm. The trend and its uncertainty is 3.11 ± 0.57 ppm/yr, 1 sigma. The corresponding monthly mean Northern Hemisphere surface measurement time series shows a monthly mean X_{CO_2} of 382.95 ± 5.98 ppm with a seasonal amplitude of 5.16 ± 0.22 ppm. The fit to the surface monthly mean time series from 17 Northern Hemisphere stations indicates a trend of 2.22 ± 0.14 ppm/yr, 1 sigma. The ACE Southern Hemisphere 7–10 km mean and uncertainty of 414.90 ± 6.40 ppm is consistent with the ACE Northern Hemisphere result. The seasonal cycle amplitude and uncertainty given by ACE for Southern Hemisphere is 4.12 ± 1.03 ppm.

[30] AIRS measurements from very clear ocean-only scenes in both hemispheres between ±60° latitude over 4 years with maximum sensitivity at 2–9 km altitude (~300–800 hPa) [*Strow and Hannon*, 2008] show X_{CO_2} 3–9 ppm lower than measured in the boundary layer, and therefore the vertically averaged 7–10 km average X_{CO_2} likely also should exhibit the CO_2 rectifier effect. Analysis shows ACE sampling of minimally impacted cloud occultations, and the latitude coverage is too sparse to derive more than one layer with 0–60°N and 0–60°S latitude

Table 3. Station Codes Locations, and Altitudes of the Southern Hemisphere NOAA/ESRL Surface Stations Used in the Study

Station	Latitude (°S)	Longitude (°)	Altitude (m)
ASC	7.92	−14.42	54
BHD	41.42	174.87	80
BKT	0.20	100.32	865
CGO	40.68	144.68	97
CRZ	46.45	51.85	120
EIC	27.15	−109.45	50
SEY	4.67	55.17	3.0
SMO	14.25	−170.57	42
TDF	54.87	−68.48	20

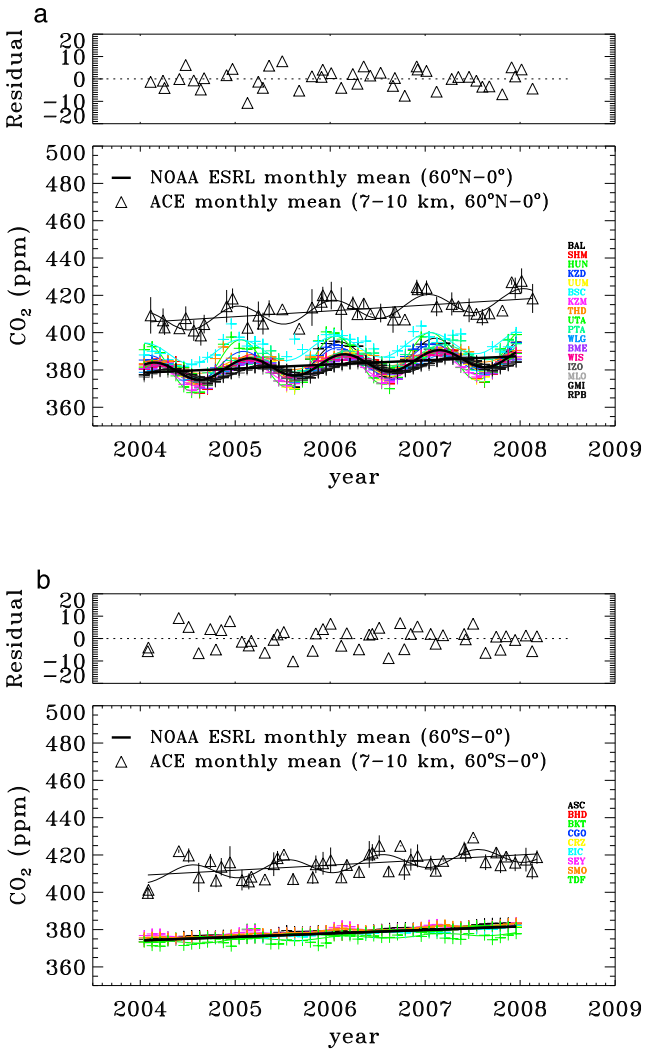

Figure 4. Comparison of monthly mean time series of ACE version 2.2 CO_2 monthly mean X_{CO_2} at 7–10 km altitude between latitudes of (a) 0–60°N latitude and (b) 0–60°S latitude with monthly mean NOAA/ESRL surface station measurements (same sites station codes as in Figure 3). The ACE monthly average measurements (open triangles) with a vertical line indicating the standard deviation have been fitted with a model that includes a sinusoidal seasonal cycle based on equation (1) (solid line). Altitude shifts have been applied to the measurements (see text for details). Measured minus calculated residuals derived with equation (1) (solid line) are shown above on an expanded vertical scale.

Table 5. Best Fit for the Seasonal Cycle Amplitude and the Month of the Peak Derived From Northern Hemisphere Surface Stations[a]

Station Latitude (°N)	Seasonal Cycle Amplitude (ppm)	Month of Peak for Seasonal Cycle
BAI (55.5)	7.82 ± 0.61	January
SHM (52.72)	7.47 ± 0.58	February
HUN (46.95)	13.28 ± 0.56	January
KZD (44.45)	7.69 ± 0.44	January
UUM (44.45)	6.71 ± 0.50	February
BSC (44.17)	6.08 ± 0.85	January
KZM (43.25)	6.21 ± 0.37	January
THD (41.05)	3.95 ± 0.63	February
UTA (39.90)	4.38 ± 0.30	February
PTA (38.95)	4.82 ± 0.65	February
WLG (36.27)	4.38 ± 0.33	February
BME (32.37)	5.55 ± 0.31	February
WIS (31.13)	4.61 ± 0.28	February
IZO (28.30)	3.47 ± 0.20	March
MLO (19.53)	3.29 ± 0.14	April
GMI (13.43)	3.06 ± 0.13	April
RPB (13.17)	3.63 ± 0.16	March

[a]Date corresponding to the seasonal maximum was determined from a fit based on equation (1).

averages required to retain a sufficient number of occultations to accurately quantify trends and the difference in the seasonal cycles in the two hemispheres.

[31] We have used the regression fit obtained from the third term on the right side of equation (1) to determine the amplitude of the seasonal cycle for each Northern Hemisphere surface station and the month corresponding to the seasonal maximum. We limit our comparison to the Northern Hemisphere as the amplitude of the seasonal cycle is small in the Southern Hemisphere [*Erickson et al.*, 1996, Figure 3]. The results for the Northern Hemisphere stations are given in Table 5. The month of the seasonal maximum from the Northern Hemisphere surface stations occur between January and April. The amplitude of the monthly average seasonal cycle is observed to generally increase with increasing latitude (~3 ppm in the subtropics to ~8 ppm at high latitudes) except for the HUN station at 46.95°N (amplitude of 13.28 ± 0.56 ppm). The majority of those amplitudes are in the range 3–6 ppm, consistent with the peak-to-peak seasonal variations of 6–8 ppm determined from upper tropospheric Northern Hemisphere aircraft measurements [*Nakazawa et al.*, 1991; *Sawa et al.*, 2008] and ground-based total column measurements from Kitt Peak, which showed an average seasonal variation

Table 4. Best Fit Parameters[a]

Case	Mean VMR (ppm)	VMR Trend (ppm/yr)	Trend (% yr^{-1})	Seasonal Cycle Amplitude (ppm)	NMO	NMS
A	412.35 ± 7.20	3.11 ± 0.56	0.77 ± 0.14	5.60 ± 0.92	44	333
B	414.90 ± 6.40	2.75 ± 0.61	0.67 ± 0.15	4.12 ± 1.03	46	455
C	382.95 ± 5.98	2.22 ± 0.14	0.59 ± 0.04	5.16 ± 0.22		
D	378.05 ± 2.62	1.87 ± 0.07	0.50 ± 0.02	0.10 ± 0.09		

[a]Cases are A, monthly mean ACE Northern Hemisphere (0–60°N) latitude 7–10 km altitude; B, ACE Southern Hemisphere (0–60°S) 7–10 km altitude; C, NOAA/ESRL Northern Hemisphere surface; and D, Southern Hemisphere surface CO_2 time series for the February 2004 to March 2008 time period. Altitude-shifted monthly mean ACE occultations fit with equation (1). NMO and NMS are the number of measurement months and the number of valid occultations after excluding cloudy and/or aerosol-impacted ACE measurements, respectively. Monthly mean NOAA/ESRL Northern Hemisphere (17 stations) (case C) and Southern Hemisphere (9 stations) (case D) were used to infer surface trends and seasonal cycle amplitudes.

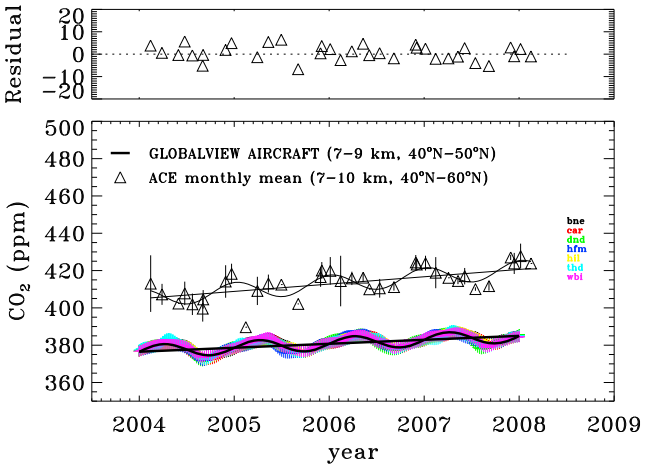

Figure 5. Comparisons of ACE 40–60°N latitude monthly average altitude-shifted measurements results and a best fit to that time series with the corresponding results from GLOBALVIEW model weekly time series for seven locations near 40°N. The format for the ACE measurements is the same as in Figures 3 and 4 and both ACE and model time series cover the same time period (2004–2008) with equation (1) used to fit the time series. The station code for each GLOBALVIEW site (http://www.esrl.noaa.gov/gmd/ccgg/globalview/) is also displayed. The ACE seasonal cycle maximum occurs in the middle of January with an amplitude 1.158 ± 031%. The month of seasonal cycle maximum for GLOBALVIEW is found to occur in April, and the amplitude is 0.92 ± 0.01%. A total of 36 monthly means from ACE observations of 217 occultations are included in the analysis.

peak-to-peak amplitude of 7 ppm [*Yang et al.*, 2002]. The 4-year AIRS climatology from ocean-only clear sky scenes between 10°N to 60°N latitude with maximum sensitivity to CO_2 variability at 300–800 hPa (3–9 km) [*Strow and Hannon*, 2008] also reported an average seasonal amplitude of 3 ppm.

[32] Figure 5 compares ACE 40–60°N latitude monthly average results with results from GLOBALVIEW model weekly time series for seven ground station locations between 40°N and 50°N. The format for the ACE measurements is the same as in Figures 3 and 4, and both ACE measurements and model predictions cover the same time period (2004–2008). Equation (1) was used to fit time series of both data sets. The station code for each GLOBALVIEW site (http://www.esrl.noaa.gov/gmd/ccgg/globalview/) is also displayed. The ACE-derived seasonal cycle maximum occurs in the middle of January with an amplitude 1.158 ± 0.31%. The month of seasonal cycle maximum for GLOBALVIEW is found to occur in April, and the amplitude is 0.92 ± 0.01%. A total of 36 monthly means from ACE observations of 217 occultations are included in the analysis.

[33] The GLOBALVIEW predictions are derived from NOAA middle and upper tropospheric aircraft measurements and are described as having been smoothed, interpolated, and extrapolated. The ACE X_{CO_2} measurements are higher than those predicted by GLOBALVIEW, and the phase and amplitude of the seasonal cycle maxima as well as the X_{CO_2} trend are all different. As the GLOBALVIEW database is widely used and has been included in validation studies [see, e.g., *Strow and Hannon*, 2008, Figure 9], it is an important database, but it is not possible to determine if the differences between ACE results and GLOBALVIEW predictions for trend or seasonal cycle amplitude and phase are real or artifacts.

[34] Table 6 provides a listing of ACE monthly average measurements (and standard deviations), a best fit obtained to the time series with equation (1), the latitude range, and the number of occultations in Northern Hemisphere for each

Table 6. Measured, Best Fit Calculated, Latitude Range, Number of Occultations From ACE Northern Hemisphere Monthly Averaged Measurements Between February 2004 and February 2008[a]

Date (Year and Month)	CO_2 Monthly Average ± SD (ppm)	Regression Fit CO_2	Latitude Range (°N)	NMOC
2004 Feb	409.25 ± 9.79	410.58	8.3–58.78	11
2004 Mar	406.56 ± 6.42	407.35	35.92–59.46	23
2004 Apr	402.78 ± 3.98	406.85	19.75–35.64	9
2004 May	402.35 ± 0.0	402.42	57.95	1
2004 Jun	407.77 ± 6.29	401.55	51.16–51.72	5
2004 Jul	401.10 ± 5.57	401.78	33.9–58.33	25
2004 Aug	398.48 ± 5.42	403.21	4.34–43.35	19
2004 Sep	404.57 ± 4.99	404.23	44.47–56.34	11
2004 Nov	414.15 ± 8.71	412.49	53.88–59.26	7
2004 Dec	418.26 ± 5.40	413.77	41.37–55.44	10
2005 Feb	402.62 ± 11.44	413.34	8.89–58.71	3
2005 Mar	409.28 ± 7.88	410.36	42.42–58.24	12
2005 Apr	404.82 ± 5.85	408.80	4.87–32.92	17
2005 May	412.76 ± 4.57	406.84	35.25–59.25N	9
2005 Jun	412.48 ± 0.0	404.57	44.08	1
2005 Sep	402.13 ± 0.37	407.36	47.07–47.69	2
2005 Oct	413.47 ± 9.85	412.29	17.88–36.35	5
2005 Nov	416.54 ± 5.25	415.60	55.53–59.94	7
2005 Dec	420.07 ± 4.49	415.92	50.42–54.53	3
2006 Jan	419.86 ± 7.38	417.27	56.57–59.28	7
2006 Feb	412.70 ± 11.58	416.68	4.79–58.69	7
2006 Mar	415.80 ± 3.59	413.61	54.95–59.96	4
2006 Apr	409.90 ± 2.31	412.05	17.31–39.38	11
2006 May	415.66 ± 2.37	410.06	30.68–58.98	5
2006 Jun	409.98 ± 0.0	408.46	54.76	1
2006 Jul	410.50 ± 5.01	407.72	48.57–55.44	5
2006 Aug	406.99 ± 7.08	410.09	9.98–35.54	2
2006 Sep	411.14 ± 1.91	410.72	43.15–56.67	7
2006 Oct	407.03 ± 0.0	414.53	24.03	1
2006 Nov	424.37 ± 3.98	418.76	56.71–59.25	5
2006 Dec	423.25 ± 3.30	419.01	53.32–56.49	6
2007 Jan	423.99 ± 3.97	420.39	53.91–59.91	9
2007 Feb	414.05 ± 5.26	419.72	1.47–57.84	12
2007 Apr	415.39 ± 6.18	415.39	8.06–41.25	7
2007 May	414.14 ± 1.41	413.26	26.94–58.90	6
2007 Jun	411.96 ± 6.36	411.00	38.93–57.64	4
2007 Jul	410.09 ± 0.94	410.87	49.37–52.23	2
2007 Aug	408.24 ± 4.36	411.715	17.52–37.83	7
2007 Sep	410.33 ± 2.73	413.65	34.35–55.05	11
2007 Oct	411.83 ± 0.0	418.67	26.15	1
2007 Nov	427.04 ± 1.38	421.85	58.46–59.97	3
2007 Dec	423.83 ± 5.66	422.69	47.35–56.99	10
2008 Jan	427.75 ± 6.68	423.50	52.55–59.78	18
2008 Feb	418.32 ± 7.77	422.63	22.45–51.12	2

[a]The best fit calculated CO_2 VMRs were obtained from a fit to the time series with equation (1). NMOC is the number of number of valid occultations after excluding cloudy and/or aerosol-impacted ACE measurements and those inside or on the edge of the polar vortex. See text for details.

Table 7. Measured, Best Fit Calculated, Latitude Range, Number of Occultations From ACE Southern Hemisphere Monthly Averaged Measurements Between February 2004 and March 2008[a]

Date (Year and Month)	CO_2 Monthly. Average ± SD (ppm)	Regression Fit CO_2	Latitude Range (°S)	NOCC
2004 Feb	401.34 ± 0.0	405.323	23.44	1
2004 May	422.05 ± 0.91	412.867	58.19–58.94	4
2004 Jul	419.73 ± 3.79	414.490	55.80–59.22	6
2004 Aug	407.94 ± 7.81	414.431	1.44–21.48	4
2004 Sep	416.71 ± 3.84	412.447	43.04–59.99	14
2004 Oct	406.25 ± 3.57	411.095	9.31–38.74	24
2004 Nov	413.67 ± 4.70	409.847	39.24–59.91	42
2004 Dec	416.07 ± 8.66	408.274	43.64–52.51	6
2005 Jan	406.54 ± 5.53	407.946	27.92–58.12	22
2005 Feb	405.80 ± 4.25	408.882	14.74–40.03	10
2005 Mar	408.37 ± 0.65	409.398	41.49–41.73	2
2005 Apr	406.87 ± 0.76	413.178	2.07–7.30	3
2005 May	415.06 ± 6.37	415.612	58.86–59.94	8
2005 Jun	418.52 ± 4.11	416.272	39.31–53.07	7
2005 Jul	419.72 ± 0.0	417.270	58.00	1
2005 Aug	407.11 ± 3.24	417.235	5.29–14.23	2
2005 Oct	407.95 ± 3.51	413.416	3.84–32.56	14
2005 Nov	415.00 ± 4.74	412.697	33.3–58.47	31
2005 Dec	415.54 ± 6.12	411.300	34.19–56.82	10
2006 Jan	417.20 ± 6.81	410.560	56.51–59.35	4
2006 Feb	408.01 ± 2.47	411.206	6.93–34.78	17
2006 Mar	414.66 ± 2.85	412.284	37.75–56.41	8
2006 Apr	410.90 ± 3.32	415.709	9.24–26.55	6
2006 May	420.28 ± 7.17	418.502	55.85–59.61	9
2006 Jun	421.24 ± 4.56	419.142	49.09–50.03	7
2006 Jul	424.89 ± 5.64	420.045	53.13–59.99	8
2006 Aug	411.23 ± 2.71	419.937	12.62–25.65	8
2006 Sep	424.89 ± 0.0	417.964	59.36	1
2006 Oct	412.48 ± 5.67	417.042	6.54–47.79	20
2006 Nov	417.53 ± 5.90	415.444	29.73–58.47	22
2006 Dec	419.54 ± 6.14	414.121	55.19–58.68	4
2007 Jan	415.44 ± 4.14	413.375	34.8–58.75	16
2007 Feb	411.56 ± 2.14	413.885	15.43–32.03	3
2007 Mar	416.81 ± 0.0	415.333	56.56	1
2007 May	423.31 ± 3.81	421.244	57.71–59.93	4
2007 Jun	421.25 ± 5.01	421.572	50.55–54.58	4
2007 Jul	429.36 ± 0.0	422.711	52.51	1
2007 Aug	416.11 ± 4.21	422.476	3.15–27.39	5
2007 Sep	421.37 ± 2.91	420.479	50.83–51.96	3
2007 Oct	414.49 ± 4.20	419.451	0.56–46.54	13
2007 Nov	419.16 ± 2.46	418.114	33.54–59.55	9
2007 Dec	415.87 ± 4.54	416.501	34.61–59.69	16
2008 Jan	417.50 ± 6.35	416.138	35.68–58.72	25
2008 Feb	411.22 ± 4.21	416.867	3.90–33.25	17
2008 Mar	419.04 ± 3.81	417.847	34.95–57.29	9

[a]The best fit calculated CO_2 VMRs were obtained from a fit to the time series with equation (1). NMOC is the number of number of valid occultations after excluding cloudy and/or aerosol-impacted ACE measurements and those inside or on the edge of the polar vortex. See text for details.

month from the February 2004 to February 2008 time period. Table 7 provides a listing of the same information in the same format from the Southern Hemisphere 0–60°S measurements. It can be noted that the fit to the seasonal variation is not as good for the Southern Hemisphere results as those from the Northern Hemisphere.

[35] The X_{CO_2} rectifier effect noted earlier [*Strow and Hannon*, 2008] indicates X_{CO_2} in the lower mean troposphere is several parts per million lower than in the boundary layer near the same site for the same time period. Higher CO_2 ACE measurements at 7–10 km are also inconsistent with model profile calculations for the Mauna Loa station [*Erickson et al.*, 1996, Figure 11] and upper tropospheric aircraft measurements [*Nakazawa et al.*, 1991; *Sawa et al.*, 2008].

6. Summary and Conclusions

[36] Retrievals of X_{CO_2} have been performed for February 2004 to March 2008 at 0–60°N and 0–60°S latitudes from ACE SCISAT-1 spectra based on an analysis procedure that is described in section 3. Monthly average X_{CO_2} retrieved from the ACE-FTS spectra at 7–10 km are higher on average by a factor of 1.07 ± 0.025 in the Northern Hemisphere and by a factor of 1.09 ± 0.019 in the Southern Hemisphere than NOAA ESRL surface station measurements covering the same time span. The ACE-derived trend is also ~1 ppm per year (0.2% yr^{-1}) higher than measured at those surface stations during the same observation period. A bias between remote sensing and correlative measurements has been reported previously [*Yang et al.*, 2002; *Bösch et al.*, 2006], with offsets of several percent between the different measurement sets identified. Different biases were reported for the two CO_2 channels used for retrievals by the AIRS instrument [*Strow and Hannon*, 2008]. Therefore, there is a need for further laboratory studies of CO_2 in both the visible and infrared to reduce systematic sources of error. The systematic errors estimated for our results are much larger than those required to quantify the variation of sources and sinks and improve future climate forecasts. The results are also not accurate enough to infer surface fluxes given the high precision needed for space-based measurements [*Miller et al.*, 2007]. Additional low-temperature measurements are planned and may reduce the uncertainty in the N_2 continuum absorption coefficients, including the atmospheric window region near 2500 cm^{-1}.

[37] The ACE X_{CO_2} measurements is inconsistent with the CO_2 rectifier effect reported from a 4 year climatology of AIRS lower tropospheric clear sky ocean-only satellite measurements [*Strow and Hannon*, 2008] and a decrease with altitude in X_{CO_2} predicted above Mauna Loa [*Erickson et al.*, 1996]. ACE measurements at 40–60°N latitude have been compared with NOAA-ESRL surface station measurements for a 36 month time period and exhibit agreement in the time of the seasonal cycle peak within 1 month. ACE X_{CO_2} measurements have also been compared with values predicted for the same time span based on the GLOBALVIEW aircraft database. The phase and amplitude of the seasonal cycle as well as the trend for X_{CO_2} differ from those measured by ACE. As indicated in Figure 5, the seasonal amplitudes from ACE and GLOBALVIEW time series are found to be 4.78 and 3.51 ppm, respectively. The time of occurrence of seasonal maximum is January and April, respectively. Since GLOBALVIEW predictions represent temporal variations of localized regions (mostly over the USA) and the ACE results represent an average over the latitude range 40–60°N, certain differences are anticipated. The averaged X_{CO_2} amount from ACE is higher than GLOBALVIEW by a factor of 1.08.

[38] Our use of monthly average measurements averaged over latitude range and a 3 km wide altitude range and the need to exclude occultations impacted by clouds, aerosols, and/or descent reflect the measurement limitations from an occultation instrument such as ACE. Despite the sparse sampling, the capability of the ACE-FTS to also precisely

and simultaneously measure a comprehensive set of chemical tracers with a range of lifetimes and sources, such as CO, CH_4, HCOOH, O_3, C_2H_6, C_2H_4, HCN, CH_3OH, SF_6, OCS, and C_2H_2, offers the potential to use those measurements over land and ocean scenes in both hemispheres to differentiate air mass types and offer constraints on the factors needed in model vertical transport from surface source regions to the upper troposphere [*Law et al.*, 1996] (e.g., biomass burning, fossil fuel emissions, continental outflow as a function of latitude, season, and time). The ACE near global mid-tropospheric measurements of X_{CO_2}, and CH_4 will provide validation for those obtained by the GOSAT FTS [*Hamazaki et al.*, 2005]. ACE observations are just one of many data sets that are needed to help quantify the global atmospheric distribution of X_{CO_2}, to constrain uncertainties in its atmospheric flux budget, and improve modeling of lower to upper tropospheric transport.

[39] **Acknowledgments.** We acknowledge initial support from NASA's carbon cycle program (NRA 04-OES-01). NASA support to continue the analysis of ACE infrared spectra for both stratospheric and tropospheric composition and long-term trends is acknowledged. The ACE satellite mission is funded primarily by the Canadian Space Agency (CSA), and some support is also provided the Natural Environment Research Council (NERC) of the UK. We thank D. Fu for providing us with a list of extravortex occultations. The surface CO_2 measurements displayed in Figures 3 and 4 are freely available from NOAA/ESRL, and we acknowledge their use in this investigation. We acknowledge GLOBALVIEW CO_2: Cooperative Atmospheric Data Integration Project-Carbon Dioxide, NOAA CMDL, Boulder, Colorado. (Also available via anonymous FTP to ftp.cmdl.noaa.gov, Path: ccg/co2/GLOBALVIEW.)

References

Allison, C. E., and R. J. Francey (2007), Verifying Southern Hemisphere trends in atmospheric carbon dioxide stable isotopes, *J. Geophys. Res.*, *112*, D21304, doi:10.1029/2006JD007345.

Baranov, Y. I., W. J. Lafferty, and G. T. Fraser (2005), Investigation of collision-induced absorption in the vibrational fundamentals of N_2 and O_2, *J. Mol. Spectrosc.*, *233*, 160–163, doi:10.1016/j.jms.2005.06.008.

Bernath, P. F., et al. (2005), Atmospheric Chemistry Experiment (ACE): Mission overview, *Geophys. Res. Lett.*, *32*, L15S01, doi:10.1029/2005GL022386.

Boone, C. D., R. Nassar, K. A. Walker, Y. Rochon, S. D. McLeod, C. P. Rinsland, and P. F. Bernath (2005), Retrievals for the Atmospheric chemistry experiment Fourier-transform spectrometer, *Appl. Opt.*, *44*, 7218–7231, doi:10.1364/AO.44.007218.

Bösch, H., et al. (2006), Space-based near-infrared CO_2 measurements: Testing the Orbiting Carbon Observatory retrieval algorithm and validation concept using SCIAMACHY observations over Park Falls, Wisconsin, *J. Geophys. Res.*, *111*, D23302, doi:10.1029/2006JD007080.

Buchwitz, M., O. Schneising, J. P. Burrows, H. Bovensmann, M. Reuter, and J. Notholt (2007), First direct observation of the atmospheric CO_2 year-to-year increase from space, *Atmos. Chem. Phys.*, *7*, 4249–4256.

Carlotti, M. (1988), Global fit approach to the analysis of limb-scattering atmospheric measurements, *Appl. Opt.*, *27*, 3250–3254, doi:10.1364/AO.27.003250.

Chahine, M. T., L. Chen, P. Dimotakis, X. Jiang, Q. Li, E. T. Olsen, T. Pagano, J. Randerson, and Y. L. Yung (2008), Satellite remote sounding of mid-tropospheric CO_2, *Geophys. Res. Lett.*, *35*, L17807, doi:10.1029/2008GL035022.

Chevallier, F., R. J. Engelen, and P. Peylin (2005), The contribution of AIRS data to the estimation of CO_2 sources and sinks, *Geophys. Res. Lett.*, *32*, L23801, doi:10.1029/2005GL024229.

Connor, B. J., A. Parris, J. J. Tsou, and M. P. McCormick (1995), Error analysis for the ground-based microwave measurements during STOIC, *J. Geophys. Res.*, *100*, 9283–9291, doi:10.1029/94JD00413.

Crisp, D., et al. (2004), The Orbiting Carbon Observatory (OCO) mission, *Adv. Space Res.*, *34*(4), 700–709, doi:10.1016/j.asr.2003.08.062.

De Bièvre, P., M. Gallet, N. E. Holden, and I. L. Barnes (1984), Isotopic abundances and atomic weights of the elements, *J. Phys. Chem. Ref. Data*, *13*, 809–891.

Erickson, D. J., III, P. J. Rasch, P. P. Tans, P. Friedlingstein, P. Ciais, E. Maier-Reimer, K. Six, C. A. Fischer, and S. Walters (1996), The seasonal cycle of atmospheric CO_2: A study based on the NCAR Community Climate Model (CCM2), *J. Geophys. Res.*, *101*, 15,079–15,097, doi:10.1029/95JD03680.

Fan, S., M. Gloor, J. Mahlman, S. Pacala, J. Sarmiento, T. Takasahi, and P. Tans (1998), A large terrestrial carbon sink in North America implied by atmospheric and oceanic CO_2 data and models, *Science*, *282*, 442–446, doi:10.1126/science.282.5388.442.

Foucher, P. Y., A. Chédin, G. Dufour, V. Capelle, C. D. Boone, and P. Bernath (2009), Technical note: Feasibility of CO_2 profile retrieval from limb viewing solar occultation made by the ACE-FTS instrument, *Atmos. Chem. Phys.*, *9*, 2873–2890.

Francey, R. J., and P. P. Tans (1987), The latitudinal variation in oxygen-18 of atmospheric CO_2, *Nature*, *327*, 495–497, doi:10.1038/327495a0.

Hamazaki, T., Y. Kaneko, A. Kuze, and K. Kondo (2005), Fourier transform spectrometer for Greenhouse Gases Observing Satellite (GOSAT), *Proc SPIE*, *5659*, 73–80, doi:10.1117/12.581198.

Hoke, M. L., and J. H. Shaw (1982), Analysis of CO_2 bands near 3.6 μm, *Appl. Opt.*, *21*, 929–934, doi:10.1364/AO.21.000929.

Intergovernmental Panel on Climate Change (2007), *Climate Change 2007: The Physical Science Basis*, Geneva.

Kent, G. S., P.-H. Wang, M. P. McCormick, and K. M. Skeens (1995), Multiyear stratospheric aerosol and gas experiment II measurements of upper tropospheric aerosol characteristics, *J. Geophys. Res.*, *100*, 13,875–13,899, doi:10.1029/95JD00017.

Lafferty, W. J., A. M. Solodov, A. Weber, W. B. Olson, and J.-M. Hartmann (1996), Infrared collision-induced absorption by N_2 near 4.3 μm for atmospheric applications: Measurements and empirical modeling, *Appl. Opt.*, *35*, 5911–5917, doi:10.1364/AO.35.005911.

Law, R. M., et al. (1996), Variations in modeled atmospheric transport of carbon dioxide and the consequences for CO_2 inversions, *Global Biogeochem. Cycles*, *10*(4), 783–796, doi:10.1029/96GB01892.

Malathy Devi, M., C. P. Rinsland, and D. C. Benner (1984), Absolute intensity measurements of CO_2 bands in the 2395–2680 cm^{-1} region, *Appl. Opt.*, *23*, 4067–4075, doi:10.1364/AO.23.004067.

Menoux, V. R., Le Doucen, C. Roulet, A. Roublen, and A. M. Bouchardy (1993), Collision-induced absorption in the fundamental band of N_2: Temperature dependence of the absorption by N_2-N_2 pairs, *Appl. Opt.*, *32*, 263–268, doi:10.1364/AO.32.000263.

Miller, C. E., et al. (2007), Precision requirements for space-based X_{CO_2} data, *J. Geophys. Res.*, *112*, D10314, doi:10.1029/2006JD007659.

Nakazawa, T., K. Miyashita, S. Aoki, and M. Tanaka (1991), Temporal and spatial variations of upper tropospheric and lower stratospheric carbon dioxide, *Tellus, Ser. B*, *43*, 106–117.

Nakazawa, T., S. Sugawara, G. Inoue, T. Machida, S. Makshyutov, and H. Mukai (1997), Aircraft measurements of the concentrations of CO_2, CH_4, N_2O, and CO and the carbon and oxygen isotopic ratios of CO_2 over Russia, *J. Geophys. Res.*, *102*, 3843–3859, doi:10.1029/96JD03131.

Pak, B. C., and M. J. Prather (2001), CO_2 source inversions using satellite observations in the upper troposphere, *Geophys. Res. Lett.*, *28*, 4571–4574, doi:10.1029/2001GL013604.

Parrish, A. B. J., Connor, J. J. Tsou, I. S. McDermid, and W. P. Chu (1992), Ground-based microwave monitoring of stratospheric ozone, *J. Geophys. Res.*, *97*, 2541–2546.

Patra, P. K., S. Maksyutov, Y. Sasano, H. Nakajima, G. Inoue, and T. Nakazawa (2003), An evaluation of CO_2 observations with solar occultation FTS for inclined-orbit satellite sensor for surface source inversion, *J. Geophys. Res.*, *108*(D24), 4759, doi:10.1029/2003JD003661.

Rayner, P. J., and P. M. O'Brien (2001), The utility of remotely sensed CO_2 concentration data in surface source inversions, *Geophys. Res. Lett.*, *28*, 175–178, doi:10.1029/2000GL011912.

Rinsland, C. P., R. Zander, C. B. Farmer, R. H. Norton, and J. M. Russell III (1987), Concentrations of ethane (C_2H_6) in the lower stratosphere and upper troposphere and acetylene (C_2H_2) in the upper troposphere deduced from atmospheric trace molecule spectroscopy/Spacelab 3 Spectra, *J. Geophys. Res.*, *92*, 11,951–11,964, doi:10.1029/JD092iD10p11951.

Rinsland, C. P., R. Zander, J. S. Namkung, C. B. Farmer, and R. H. Norton (1989), Stratospheric infrared continuum absorptions observed by the ATMOS instrument, *J. Geophys. Res.*, *94*, 16,303–16,322, doi:10.1029/JD094iD13p16303.

Rinsland, C. P., et al. (1991), Stratospheric profiles of heavy water vapor isotopes and CH_3D from analysis of the ATMOS Spacelab 3 infrared solar spectra, *J. Geophys. Res.*, *96*, 1057–1068, doi:10.1029/90JD02234.

Rinsland, C. P., G. K. Yue, M. R. Gunson, R. Zander, and M. C. Abrams (1994), Mid-infrared extinction by stratospheric sulfate aerosols from the Mt. Pinatubo eruption, *J. Quant. Spectrosc. Radiat. Transf.*, *52*, 241–252, doi:10.1016/0022-4073(94)90154-6.

Rinsland, C. P., et al. (1998), ATMOS/ATLAS 3 infrared profile measurements of clouds in the tropical and subtropical upper troposphere, *J. Quant. Spectrosc. Radiat. Transf.*, *60*, 903–919, doi:10.1016/S0022-4073(98)00093-4.

Rinsland, C. P., M. J. McHugh, and F. W. Irion (2004), Lower stratospheric densities from solar occultation measurements of continuum absorption near 2400 cm^{-1}, *J. Geophys. Res.*, *109*, D01301, doi:10.1029/2003JD003803.

Rinsland, C. P., R. Nassar, C. B. Boone, P. Bernath, L. Chiou, D. Weisenstein, E. Mahieu, and R. Zander (2007), Spectroscopic detection of COClF in the tropical and mid-latitude lower stratosphere, *J. Quant. Spectrosc. Radiat. Transf.*, *105*, 467–475, doi:10.1016/j.jqsrt.2006.11.013.

Rinsland, C. P., L. S. Chiou, E. Mahieu, C. D. Boone, and P. F. Bernath (2010), First measurements of the trend of HCFC142b from Atmospheric Chemistry Experiment (ACE) solar occultation spectra, *J. Quant. Spectrosc. Radiat. Transf.*, *110*, 2127–2134, doi:10.1016/j.jqsrt2009.05.011.

Rodgers, C. D. (1990), Characterization and error analysis of profiles retrieved from remote sounding measurements, *J. Geophys. Res.*, *95*, 5587–5595, doi:10.1029/JD095iD05p05587.

Rothman, L. S., et al. (2005), The HITRAN 2004 molecular spectroscopy database, *J. Quant. Spectrosc. Radiat. Transf.*, *96*, 139–204, doi:10.1016/j.jqsrt.2004.10.008.

Sawa, Y., T. Machida, and H. Matsueda (2008), Seasonal variations of CO_2 near the tropopause observed by commercial aircraft, *J. Geophys. Res.*, *113*, D23301, doi:10.1029/2008JD010568.

Sica, R. J., et al. (2008), Validation of the Atmospheric Chemistry Experiment (ACE) version 2.2 temperature using ground-based and space-borne measurements, *Atmos. Chem. Phys.*, *8*, 35–62.

Strow, L. L., and S. E. Hannon (2008), A 4-year zonal climatology of lower tropospheric CO_2 derived from ocean-only Atmospheric Infrared Sounder observations, *J. Geophys. Res.*, *113*, D18302, doi:10.1029/2007JD009713.

Tans, P. P., I. Y. Fung, and T. Takahasi (1990), Observational constraints on the global atmospheric CO_2 budget, *Science*, *247*, 1431–1438, doi:10.1126/science.247.4949.1431.

Tans, P. P., P. S. Bakwin, and G. W. Guenther (1996), A feasible global carbon cycle observing system: A plan to decipher today's carbon cycle based on observations, *Global Change Biol.*, *2*, 309–318, doi:10.1111/j.1365-2486.1996.tb00082.x.

Tiwari, Y. K., M. Gloor, R. J. Englen, F. Chevallier, C. Rödenbeck, S. Körner, P. Peylen, B. H. Braswell, and M. Heimann (2006), Comparing CO_2 retrieved from Atmospheric Infrared Sounder with model predictions: Implications for constraining surface fluxes and lower to upper tropospheric transport, *J. Geophys. Res.*, *111*, D17106, doi:10.1029/2005JD006681.

Wang, P.-H., D. Rind, C. R. Trepte, G. S. Kent, G. K. Yue, and K. M. Skeens (1998), An empirical model study of the tropospheric meridional circulation based on SAGE II observations, *J. Geophys. Res.*, *103*, 13,801–13,818, doi:10.1029/98JD00204.

Winker, D. M., W. H. Hunt, and M. J. McGill (2007), Initial performance assessment of CALIOP, *Geophys. Res. Lett.*, *34*, L19803, doi:10.1029/2007GL030135.

Yang, Z., G. C. Toon, J. S. Margolis, and P. O. Wennberg (2002), Atmospheric CO_2 retrieved from ground-based near IR solar spectra, *Geophys. Res. Lett.*, *29*(9), 1339, doi:10.1029/2001GL014537.

P. Bernath, Department of Chemistry, University of York, Heslington, York YO10 5DD, UK. (pfb500@york.ac.uk)

C. Boone, Department of Chemistry, University of Waterloo, Waterloo, ON N2L 3G1, Canada. (cboone@sciborg.uwaterloo.ca)

L. S. Chiou, Science Systems and Applications, Inc., 10210 Greenbelt Rd., Ste. 600, Lanham, MD 20706, USA. (linda.s.chiou@nasa.gov)

C. P. Rinsland, Atmospheric Sciences Competency, NASA Langley Research Center, Mail Stop 401A, Hampton VA 23681-2199, USA. (curtis.p.rinsland@nasa.gov)